

Is a Shutdown of the Thermohaline Circulation Irreversible?

Jianjun Yin¹, Michael E. Schlesinger¹, Natasha G. Andronova¹, S. Malyshev² and B. Li¹

1. Climate Research Group, Department of Atmospheric Sciences, University of Illinois at Urbana-Champaign
2. Department of Ecology and Evolutionary Biology, Princeton University

The thermohaline circulation (THC) in the North Atlantic plays a vital role in explaining past abrupt climate changes and in maintaining the current climate. Its remarkable nonlinear dynamics, first demonstrated by Stommel, has been supported by various types of climate models. This has led to severe concerns that global warming may shut down the THC irreversibly, with consequent catastrophic climate changes, particularly for Europe. Here we use a suite of models to investigate the nonlinear response of the THC to freshwater perturbation in the northern North Atlantic. We find that the THC shuts down irreversibly in the uncoupled ocean general circulation model (OGCM) simulations, but reversibly in the coupled atmosphere/ocean general circulation model (AOGCM) simulation. This occurs because of a crucial negative feedback in the AOGCM simulation that cannot occur in the OGCM simulations. This negative feedback results from complex air-sea interactions and its operation needs detailed and comprehensive simulation about the climate system. Analysis of Stommel's 2-box ocean model supports this finding. The simulations from the uncoupled OGCM and AOGCM correspond to different parameter regimes of the 2-box model. Thus, the irreversible shutdown of the THC caused by freshwater addition appears to be a model artifact rather than a likely outcome of global warming.

1. Introduction

The importance of the Atlantic thermohaline circulation (THC) stems from its two unique properties: its huge northward heat transport and remarkable nonlinear dynamical behavior. Most previous research on the THC focused on issues related to these two properties. For example, it has been shown that the reduction of the northward heat transport induced by the shutdown of the THC can result in considerable cooling over the northern North Atlantic and surrounding regions [*Manabe and Stouffer*, 1988, 1999; *Schiller et al.*, 1997; *Rind et al.*, 2001; *Vellinga and Wood*, 2002]. If such a cooling actually occurred, it could be detrimental to the world's environment and economy. Based on contemporary climate model simulations, the Third Assessment Report of the Intergovernmental Panel on Climate Change found that this scenario cannot be completely excluded if the concentrations of greenhouse gases (GHG) continues to increase [*Cubasch et al.*, 2001].

Consideration of the possible future slowdown/shutdown of the THC requires knowledge of the dynamical behavior of the THC. The box ocean model [*Stommel*, 1961; *Titz et al.*, 2002], the zonally averaged ocean model [*Stocker and Wright*, 1991], the climate model of intermediate complexity [*Ganopolski et al.*, 2001; *Schmittner et al.*, 2001], the uncoupled OGCM [*Marotzke et al.*, 1991; *Mikolajewicz and Maier-Reimer*, 1994; *Prange et al.*, 2002] and the hybrid model [*Rahmstorf*, 1995; *Schmittner et al.*, 2002] have shown that the THC is a highly nonlinear dynamical system. In response to a sequential increase and then decrease of the freshwater input to the northern North Atlantic, the THC in these simplified models exhibits bistability, bifurcation, hysteresis and irreversibility. Such an input of freshwater into the North Atlantic Ocean is what might occur in the future as GHG emissions continue to increase, the earth warms, and freshwater is added to the northern North Atlantic by increasing the excess of precipitation over evaporation there, and by the melting of nearby sea ice, mountain glaciers and the Greenland ice sheet. Indeed, a freshening in high latitudes of the North Atlantic and an increase in salinity in low latitudes has recently been reported [*Curry et al.*, 2003; *Schmidt et al.*, 2004]. Subsequently, concern about global warming and a potential irreversible shutdown of the THC results in a decision to abatement GHG emissions to decrease the freshwater addition.

However, recent simulations with sophisticated atmosphere/ocean general circulation models (AOGCMs) obtain only a single stable mode of the THC, a linear response of the THC to the freshwater addition, and no critical forcing magnitude to trigger an abrupt transition [Schiller *et al.*, 1997; Rind *et al.*, 2001; Vellinga and Wood, 2002]. The THC tends to be relatively insensitive to the freshwater perturbation in the AOGCMs compared with the simplified models, and a larger freshwater perturbation is necessary to induce a dramatic reduction of the THC intensity. In addition, complex feedback processes in the THC system, which may be absent in the simplified model simulations, have been identified in the fully coupled AOGCM [Schiller *et al.*, 1997; Latif *et al.*, 1999; Vellinga *et al.*, 2002].

In terms of the dynamical behavior of the THC, there is a seeming discrepancy between the simulations by the simplified models and the sophisticated AOGCMs. It has been shown that different oceanic vertical diffusivity might cause different behavior of the THC in the climate model with intermediate complexity [Schmittner and Weaver, 2001], in the ocean-only model [Prange *et al.*, 2003], and in the fully coupled AOGCM [Manabe and Stouffer, 1999]. But these studies, as well as most other research on the dynamics of the THC, have been confined to one class of model, either a “simple” model or an AOGCM. Until now little work has been done to understand the dichotomous behavior of the THC between simple and complex models, and the role therein of air-sea feedback. Furthermore, the usage of various models of mixed complexity, particularly for the oceanic part, has largely concealed the reason why the THC behaves differently. These various models usually have many different treatments of physical and dynamical processes.

Accordingly, in this study we have performed corresponding simulations with our uncoupled 18-layer OGCM and with it coupled to our 11-layer AGCM. Our hypothesis is that the different representation of the air-sea feedback is a very important factor to explain the dichotomous behavior of the THC between different hierarchies of models. As far as the THC simulation is concerned, the uncoupled OGCM, which is classified as a “simple” model in this study, is exactly the same as the OCGM in the fully coupled AOGCM. The influence of model individuality is therefore eliminated. By respectively establishing the stability diagrams for these models, the reason why simple and complex models give

distinct simulations about the dynamical behavior of the THC and the role of the air-sea interaction is investigated here.

In section 2 the OGCM and coupled AOGCM are described. The results of the control and freshwater perturbation (hosing) simulations are presented and analyzed in section 3. In section 4 the two-box model of *Stommel* [1961], as generalized by *Saltzman* [2002] is used to replace the results of both the uncoupled OGCM and coupled AOGCM. Conclusions are given in section 5.

2. Model Description

The models used in the present study include an ocean general circulation model [*Han et al.*, 1984a,b; *Schlesinger et al.*, 1985] and an atmosphere general circulation model [*Wang and Schlesinger*, 1995; *Schlesinger et al.*, 1997], both of which were developed and used at Oregon State University and the University of Illinois at Urbana-Champaign (UIUC).

The UIUC 18-layer OGCM uses depth as vertical coordinate and has a 4° latitude by 5° longitude horizontal resolution. The 18 layers range in thickness from 7.6 m at the surface ocean to 835 m in the deep ocean. The OGCM is based on the primitive equations and Bryan-Cox numerical scheme [*Bryan*, 1969]. It calculates the three-dimensional fields of oceanic velocity, temperature and salinity, and the thickness of sea ice. To facilitate the integration, the ocean flow is split into a depth-independent barotropic part and a depth-dependent baroclinic part. The rigid-lid condition is used at the ocean surface to allow a long integration time step, on the order of hours. The vertical viscosity and diffusivity are calculated according to a Richardson-number-dependent scheme [*Pacanowski and Philander*, 1981]. A thermodynamic sea ice model is embedded in the 18-layer OGCM to predict sea ice thickness and coverage, using the thermodynamic equation over the ocean surface.

The standard version of the ocean-only model is run with prescribed climatological fluxes at the air-sea interface. The ocean-only model updates its boundary conditions – wind stress, heat and freshwater fluxes – every 5 days. The mixed boundary condition is also separately used for the ocean-only model as an alternative surface boundary condition. With this boundary condition, the freshwater flux from the atmosphere is prescribed and the heat

flux is calculated proportional to the difference between the prescribed atmospheric temperature and the simulated sea surface temperature. The 18-layer OGCM has been integrated for more than one thousand years with these boundary conditions.

The UIUC 11-layer troposphere/lower-stratosphere (TLS) GCM calculates the velocity, temperature, water vapor and cloud water for 11 unevenly-spaced layers in the troposphere and lower stratosphere; the surface pressure; the temperature, soil water and snow mass on land; and many other quantities, including the temperature and water-vapor content of the air near the surface, the cloud amount and cloud water and ice, rainfall and snowfall. The horizontal distribution of dependent variables in the model is staggered according to the B-grid to simulate the process of geostrophic adjustment [Arakawa and Lamb, 1977], and the model uses finite differences that conserve the total atmospheric mass, total energy under adiabatic and frictionless motion, and enstrophy (mean square vorticity) and kinetic energy for the nondivergent component of the wind field [Arakawa, 1966]. The model has a standard horizontal resolution of 4° latitude by 5° longitude and vertically extends from the earth's surface to 50 hPa. It uses normalized pressure, σ , as its vertical coordinate and has realistic geography and topography.

The adiabatic, frictionless terms in the governing prognostic equations of the TLS GCM are marched forward in time in a one-hour cycle using a combination of Matsuno and leapfrog time integration steps, with a basic time step of 6 minutes. The diabatic, frictional terms in the governing prognostic equations are calculated once per hour. A new parameterization of infrared radiation developed by Chou and Suarez [1994] was implemented into the 11-layer model by Yang *et al.* [2000] to compute absorption and emission of terrestrial radiation due to water vapor, carbon dioxide and ozone.

The 11-layer AGCM and the 18-layer OGCM have been coupled together using a serial coupling procedure. The atmospheric model and the oceanic model are integrated forward alternatively, with the models exchanging information once per day. Daily mean fluxes of heat, water and momentum at the ocean surface are calculated by the atmospheric model and passed to the oceanic model, and the sea surface temperature (SST) and sea ice thickness from the oceanic model are passed to the atmospheric model as its ocean-surface

boundary conditions. The coupled AOGCM is flux-corrected for SST and sea surface salinity (SSS) to better simulate the present climate. After the formulation and spinup of the fully coupled AOGCM, a multi-century control run has been carried out.

3. Simulation Results

3.1. The THC in the Control Climate

In this section the THC and associated oceanic features will be analyzed based on the UIUC AOGCM control run. The ocean-only model obtains similar oceanic features and will therefore not be mentioned separately. The control climate of the atmosphere simulated by the coupled model is very close to what has been described before [*Wang and Schlesinger, 1995*].

Figure 1 shows the ocean currents in the UIUC AOGCM control run. The Gulf Stream and its extension – the North Atlantic Current – are well simulated in the upper North Atlantic (Fig. 1a). These strong currents transport a large amount of seawater northward. The slow southward flow of the North Atlantic subtropical gyre provides a partial return of the seawater. At about 60°N of the North Atlantic, there is a clear convergence of upper ocean flows which results in sinking motion there. Deep convection and deep water formation are induced by intense heat loss, forming the deep ocean currents that flow all the way to the Southern Ocean (Fig. 1b). Figure 2 displays two vertical cross-sections in the North Atlantic. At 30°N, two types of circulation are present: the horizontal wind-driven gyre circulation within the upper 500 m and the vertical THC (Fig. 2a). According to mass conservation, the Gulf Stream participates in both circulations. The THC mainly consists of two western boundary currents with opposite flow directions. At 50°N, the vertical THC is the dominant circulation pattern (Fig. 2b). Both the upper ocean current and the deep ocean current become basin-wide. The deep ocean current is stronger and located at a deeper level at 50°N, indicating a gradual upwelling and weakening of the current as it flows southward. The zonally averaged meridional overturning streamfunction (shown later) confirms that the THC is simulated reasonably well in the control run.

The successful simulation of the THC is attributable to the realistic simulation of SST and SSS. A long-term stable SST and SSS are also important criteria for validating the coupled AOGCM before the performance of freshwater perturbation experiments. Figures 3 and 4 show the geographical distributions of SST and SSS from both observation and simulation. The bias of the simulated SST (Fig. 3c) is less than 0.5°C over most of the ocean. The relatively large bias at high latitudes around Antarctica is related to the sea ice simulation. In terms of the SSS simulation (Fig. 4c), it is better over the Atlantic Ocean than the Pacific and Indian Oceans. The simulated maximum SSS in the tropical Atlantic is in good agreement with observation. The Gulf Stream and the North Atlantic Current steer high salinity seawater from the subtropical region far northward into the Nordic Sea. *Manabe and Stouffer* [1988] demonstrated that without this high salinity tongue over the northern North Atlantic, a vigorous THC cannot be obtained in the coupled AOGCM.

Figure 5 plots the time series of the global-mean root-mean-square difference (RMSD) between the simulated and observed SST and SSS. The RMSD curves ensure a stable control climate during the multi-century integration period. In most years the RMSD of SST is less than 1°C , while the RMSD of SSS is about 1.3 p.s.u. (practical salinity units) after a long-term integration. The relatively large bias of the salinity occurs from the lack of direct atmospheric feedback on salinity. As shown in Fig. 4c, however, the salinity bias mainly comes from the Pacific Ocean and Indian Ocean. It is less than 0.5 p.s.u. in the Atlantic Ocean, which is good enough for the freshwater perturbation experiments. In general, the SST simulation is better in the low and middle latitudes than the high latitudes, while the SSS simulation in the Atlantic is more close to observation than in the Pacific and Indian Oceans. Both SST and SSS are stable during the multi-century integration.

3.2. Freshwater Perturbation Experiments

The freshwater perturbation experiments with the uncoupled OGCM were performed by very slowly increasing and then decreasing the external freshwater addition to the North Atlantic between $50^{\circ}\sim 70^{\circ}\text{N}$ latitudes [*Rahmstorf*, 1995]. The freshwater perturbation changes at a rate of 0.2 Sv per 1000 years (Fig. 6). Although the setup of the experiment is a transient run, the THC is always in quasi-equilibrium with the external freshwater forcing due to the

extremely slow change of the perturbation flux. To facilitate comparison with the AOGCM simulations, several steady-state runs with fixed freshwater perturbations were also carried out using the ocean-only model.

The set of the AOGCM simulations was performed for fixed freshwater addition (“hosing”) and removal (“dehosing”) rates over the same latitude band in the North Atlantic as for the OGCM-only simulations. Two groups of freshwater perturbation experiments were carried out to test the response of the THC. The first group includes three “hosing” experiments starting from the 30th year of the control run. Perturbation freshwater fluxes of 0.05, 0.1, 0.3 Sv were uniformly input into the perturbation region in separate experiments. The 110th year of the control run was chosen as the initial condition for the second group. This group consists of three “hosing” experiments (0.1, 0.3 and 0.6 Sv) and two “dehosing” experiments. Two “dehosing” experiments starting from the shutdown state of the THC which is induced by 0.6 Sv freshwater addition, include a moderate reduction of the perturbation flux from 0.6 to 0.3 Sv and the total elimination of the 0.6 Sv freshwater addition.

Figure 7 plots time evolution of the THC intensity in two groups of freshwater perturbation experiment. In the present study, the intensity of the THC is defined as the maximum meridional streamfunction value in the North Atlantic, excluding the surface layer. The curves show the following characteristics: (1) The long-term average of the THC intensity in the control run is about 18 Sv, which is consistent with the recent estimate using high-quality hydrographic data obtained during the World Ocean Circulation Experiments [*Ganachaud and Wunsch, 2000*]; (2) There is a substantial variations of the THC intensity on the decadal time scale in the control run and small freshwater perturbation (0.05 and 0.1 Sv) experiments [*Delworth et al., 1993*]. However, these variations are greatly inhibited in the large perturbation (0.3 and 0.6 Sv) experiments; (3) The weakening of the THC in response to a small freshwater perturbations such as 0.05 and 0.1 Sv is moderate and can better be detected using the long-term mean. But a large freshwater perturbation leads to a rapid and significant slowdown of the THC. The 0.6 Sv perturbation flux is sufficient to shut down the THC; (4) The response time of the THC to the large freshwater perturbations is on the order of 50 years, which is a much shorter time scale in comparison with the

advection process of the deep ocean. It has been shown that the anomalies of the THC can propagate from the high latitudes of the North Atlantic to the equator on a time scale of months by stimulating Kelvin and Rossby waves in the ocean [Johnson and Marshall, 2002]. In the small perturbations experiments, the response time of the THC intensity is relatively longer; (5) The most important result for the 0.6 Sv freshwater perturbation experiment is that once the perturbation is reduced, the THC immediately starts recovering. Like the shutdown process, the start-up process is also fast and can be completed within about 50 years. For the “dehosing” experiment in which the perturbation is totally eliminated, the THC basically re-intensifies to the original strength.

3.3. The Dynamical Behavior of the THC

In this section the dynamical behaviour of the THC will be investigated based on the freshwater perturbation experiments. Figures 8a and 8b show the strength of the THC as a function of the freshwater added and then removed from the North Atlantic as simulated by the uncoupled OGCM with two commonly used boundary conditions: (a) prescribed heat and freshwater fluxes from the atmosphere, and (b) calculated heat and prescribed freshwater fluxes from the atmosphere (mixed boundary condition). Both simulations display similar and notable features: (1) There is a pronounced hysteresis loop in which the THC, after shutdown, can be restarted only after the freshwater addition is eliminated and changed into a freshwater extraction; (2) Three equilibria of the THC coexist under the present-day freshwater forcing. Points A and E correspond to two active THC modes whereas point C is an inactive THC mode. The different intensity between points A and E is caused by the switch on and off of the deep convection in the Labrador Sea; (3) Points B and D are thresholds along the hysteresis curves. Beyond these critical points, the THC undergoes rapid transition between the active and inactive modes. All of these features indicate a remarkable nonlinearity of the THC in the ocean-only model, which results from the domination by the positive feedbacks in the THC system. Because the mixed boundary condition eliminates the temperature-advection feedback operating to stabilize the active THC and destabilize the inactive THC, the entire hysteresis loop of Fig. 8b is shifted toward the left in comparison with Fig. 8a. This irreversibility of the THC shutdown, if true, would warrant the use of precaution in formulating GHG policy.

Figure 8c shows the strength of the THC as a function of the increase (red points) and then decrease (blue points) in freshwater added to the North Atlantic as simulated by the fully coupled AOGCM. In contrast to the uncoupled OGCM, the AOGCM does not produce a hysteresis loop when the freshwater added to the North Atlantic is increased until shutdown occurs and is then reduced. Instead, once the freshwater addition is reduced from its shutdown value, the THC restarts. Furthermore, the relation between the THC intensity and the change in freshwater addition is roughly linear throughout the entire range of freshwater addition. It can also be seen that the freshwater addition required to shut down the THC is much larger for the AOGCM than for the uncoupled OGCM.

Figure 9 compares the evolution of the meridional overturning streamfunction, which shows the rotational part of the velocity field, in the Atlantic simulated by the uncoupled OGCM and AOGCM. The top two panels (Figs. 9a and 9f) display the streamfunction patterns of the control run. It is apparent that sinking motion takes place between 50~60°N. There is an intense interhemisphere exchange of seawater mass associated with the THC, making the heat transport in the Atlantic Ocean uniformly northward. Beneath the THC cell, a counter-clockwise bottom circulation exists. In response to a 0.1 Sv increase in freshwater forcing, the THC cell in the OGCM weakens by 30% but the circulation pattern keeps intact (Fig. 9b). However, a 0.2 Sv increase in freshwater forcing causes the THC to collapse (Fig. 9c). The THC remains inactive after the 0.2 Sv is reduced (Fig. 9d) and removed (Fig. 9e). In contrast, when the freshwater perturbation is removed in the AOGCM, the THC re-intensifies from the shutdown mode (Fig. 9h) to the original active mode (Fig. 9j). Hence, the THC simulated by an ocean general circulation model responds very differently depending on whether it is uncoupled or coupled to an atmosphere general circulation model, with the former giving an irreversible THC shutdown and the latter giving a reversible THC shutdown.

3.4. A Crucial Negative Feedback

It is important to examine the reason why the THC in the fully coupled AOGCM has a different dynamical behaviour compared with in the uncoupled OGCM. The THC is driven by oceanic convection in the high latitudes of the North Atlantic. A high potential density of the surface seawater is a prerequisite for the occurrence of deep convection. Hence, the

different behavior of the THC implies a different response of the surface seawater density to the freshwater perturbation.

To analyze the surface seawater density anomalies, Figure 10 plots a T-S diagram to illustrate the response of SST and SSS in high latitudes of the North Atlantic to freshwater perturbation. For the ocean-only model (blue and green points), there is a roughly linear relation between the responses and the magnitude of the perturbation flux less than 0.1 Sv. The responses of SST and SSS become much intense beyond 0.1 Sv. The 0.2 Sv perturbation flux has reduced the SSS to a very low value, close to 30 p.s.u. in both versions of the uncoupled OGCM. Due to the usage of different thermal boundary conditions, the two versions of the uncoupled OGCM give quite different SST simulations: one is constrained to the climatological SST and the other is free to change. Considering the similar hysteresis loops given by both versions of the uncoupled OGCM, it can be deduced that SSS rather than SST over the perturbation region is the key in determining the dynamical behaviour of the THC. Unlike the ocean-only model, the coupled AOGCM always simulates an intense and roughly linear response of the SSS to the freshwater perturbation (red points). Accordingly, there must be some process operating to compensate the salinity decrease induced by the freshwater perturbation in the AOGCM.

In the uncoupled OGCM, the salinity of the upper ocean in the perturbation region decreases in response to the freshwater input, and the resulting decrease in salinity spreads over the entire North Atlantic (Fig. 11a). The salinity of the upper ocean in the AOGCM also decreases in response to the freshwater addition, but the resulting decrease in salinity is confined to the high-latitude region (Fig. 11b). This occurs because of a negative feedback in the AOGCM. Over the low-latitude Atlantic, along the route of the upper THC branch, the salinity increases in the AOGCM as a result of enhanced evaporation there and a southward shift of the Atlantic intertropical convergence zone (ITCZ) when the THC slows down in response to the high-latitude perturbation.

The enhanced evaporation results from the oceanic heat accumulation in low latitudes after the THC shutdown. This oceanic heat is originally transported by the THC to the high latitudes of the North Atlantic. The southward shift of the ITCZ is caused by a southward

movement of the Hadley circulation as a result of the SST decrease over the high-latitude North Atlantic and the SST increase over the South Atlantic [Dong and Sutton, 2002]. Figure 12 shows the changes of precipitation (P), evaporation (E) and precipitation minus evaporation (P–E) after the shutdown of the THC in the AOGCM simulation. The dipole feature over the tropical Atlantic (Fig. 12c) is clear evidence of the southward shift of the Atlantic ITCZ. The negative P–E anomalies over the low latitudes of the North Atlantic enhance the SSS there. Consequently, seawater with higher salinity is transported northward by the gyre circulation and oceanic diffusion process from the low-latitude Atlantic and compensates the initial salinity decrease over much of the perturbation region.

Figure 13 shows the zonally averaged salinity change in the Atlantic Ocean after the shutdown of the THC. For the uncoupled OGCM, a freshwater cap with negative salinity anomalies greater than 4 p.s.u. is formed in the upper North Atlantic in response to the freshwater input (Figs. 13a and 13b). The freshwater cap spreads southward to the equator. The salinity anomalies become positive south of equator. In contrast, the positive salinity anomalies in the upper Atlantic extend far northward to about 40°N in the AOGCM simulation (Fig. 13c). The freshwater cap is confined to 50~60°N. Due to the small decrease in salinity over the sinking region and the high salinity seawater close to the perturbation region, deep convection is more easily resumed in the AOGCM than in the OGCM after its cessation. Therefore, this air-sea feedback greatly weakens the stability of the inactive mode of the THC in the AOGCM simulation. Since the surface freshwater flux is prescribed in the OGCM for both types of atmospheric boundary conditions, this negative feedback cannot be simulated by the uncoupled OGCM.

Previous research based on “simple” models has emphasized the positive salinity-advection feedback inherent in the THC: the enhanced (reduced) northward salinity transport induced by an intensified (weakened) THC strengthens (weakens) the THC further [Stommel, 1961]. However, the present study shows that the air-sea interaction over the low-latitude Atlantic can generate a negative feedback to stabilize the active THC through salinity advection. In this process the transport by the gyre circulation and oceanic diffusion can be important, especially when the THC is greatly reduced or shut down. Figures 11a and 11b display clearly the spread by the wind-driven circulation and the diffusion process of a

positive salinity anomaly in the AOGCM and a negative salinity anomaly in the OGCM over the North Atlantic in comparison with the control runs. Thus, the dynamical behaviour of the THC is by far more complex in the fully coupled model than the “simple” models.

4. Analysis of Stommel’s 2-box Ocean Model

The classic two-box ocean model of *Stommel* [1961] is the simplest possible way to study the THC. The highly nonlinear dynamical behavior and the irreversible shutdown of the THC were first demonstrated using this two-box model. Analysis of the two-box ocean model may give a straight and concise understanding about the underlying mechanism and it is thus helpful to interpret the results from more sophisticated climate models such as the GCMs in the present study. Due to its highly simplification, however, the two-box ocean model is unlikely to explain perfectly the different simulations about the THC dynamics between the ocean-only model and the AOGCM. Our main purpose is to show that the reversible shutdown of the THC also can happen in the two-box ocean model. The simulations from the ocean-only model and the AOGCM may correspond to different parameter regimes of the two-box model. Here we use an improved version of the two-box ocean model by *Saltzman* [2002] in which the contribution of the wind-driven gyre circulation and eddies to the mass exchange between the equatorial and polar boxes is taken into account. Analysis results from other extensions of this model have also been presented previously [*Shaffer and Olsen*, 2001; *Alley et al.*, 2003].

The governing equation of the Stommel/Saltzman 2-box ocean model for nondimensional variables is

$$\frac{ds}{dt^*} = \Pi - |1 - s| s - Ks \quad , \quad (1)$$

where s is the difference in salinity between the equatorial and polar boxes, t^* is time, Π is the freshwater addition, and K is the ratio of the transport coefficient for the gyre circulation and eddies, k_ϕ , to that for the THC, k_ψ ; the K term was absent from the original Stommel model. The maximum streamfunction of the THC is

$$\Psi = k_{\psi} \mu_T \delta T^* (1-s) \quad , \quad (2)$$

where μ_T is the thermal volume expansion coefficient, and δT^* is the temperature difference between the equatorial and polar boxes, taken to be constant.

At equilibrium,

$$0 = \Pi - |1-s|s - Ks \quad . \quad (3)$$

There are two equilibria for $s < 1$, for which the temperature effect on density dominates the salinity effect and there is sinking in high latitudes; the first is stable,

$$s^{(1)} = \frac{1}{2} \left[(1+K) - \sqrt{(1+K)^2 - 4\Pi} \right] \quad , \quad (4)$$

and the second is unstable,

$$s^{(2)} = \frac{1}{2} \left[(1+K) + \sqrt{(1+K)^2 - 4\Pi} \right] \quad . \quad (5)$$

There is another equilibrium for $s > 1$, for which the salinity effect on density dominates the temperature effect and there is sinking in low latitudes,

$$s^{(3)} = \frac{1}{2} \left[(1-K) + \sqrt{(1-K)^2 + 4\Pi} \right] \quad , \quad (6)$$

that is, the THC reverses. Our uncoupled OGCM and at least one AOGCM [Schiller *et al.*, 1997] do produce a weak reversed THC.

Figure 14a shows the equilibrium THC streamfunction Ψ versus freshwater addition Π for different values of parameter K – the ratio of the transport coefficient for the gyre circulation and eddies to that for the THC. The THC exhibits sharply different behavior for different values of K . For $K=0$ – the case examined by Stommel [1961] – there is an unstable equilibrium circulation ($s^{(2)}$) connecting two stable equilibrium circulations, one

with sinking in high latitudes and upwelling in low latitudes ($s^{(1)}$), and another that is reversed ($s^{(3)}$). K equal to zero indicates a purely thermohaline flow in the model. In this case the THC presents pronounced bistability and strong hysteresis behavior (Fig.14b). The critical freshwater forcing (the saddle-node bifurcation point) to shut down the THC is relatively small. As K increases from zero to unity – the region examined by *Saltzman* [2002] – the region of the bistability shrinks and the hysteresis behavior becomes weaker. Larger values of Π are required for all $\Psi < 1$. When K takes the value of unity, the unstable equilibrium circulation disappears, and the two stable equilibrium circulations merge. In this case, the flow between the two boxes is the combination of wind-driven flow and thermohaline flow. The contribution of the wind-driven flow to the poleward salinity transport is significant. As K is increased above unity – a case heretofore not examined – still larger values of Π are required for all $\Psi < 1$, and the discontinuity in slope between the two stable circulations decreases. The curve gradually approaches a straight line with increasing K . Mathematically, the relatively small second term in Eq. (1) can be ignored when K takes large values. The equation becomes linear between s and Π , and between Ψ and Π . In this case, the contribution of the wind-driven flow to the mass exchange dominates that of the thermohaline flow.

The different THC behavior for different values of K results from the distinct dynamical properties of the wind-driven flow and the thermohaline flow. The thermohaline flow is generated by the south-north density (salinity) difference. This flow, in turn, feeds back on the south-north density (salinity) difference. The positive feedback inherent in the thermohaline flow essentially stems from this mutual promotion. This strong positive feedback makes the THC a self-sustaining system, in which bistability and hysteresis behavior could easily be generated. However, the wind-driven flow is not induced by the north-south density difference. But it still can affect the north-south salinity difference by transporting high-salinity seawater poleward. So, the positive feedback does not exist in the wind-driven flow. Figure 14a implies that if the contribution of the wind-driven flow to the poleward salinity transport is significant (K takes large value), the nonlinear behavior of the THC could be greatly suppressed.

Figure 14b shows Ψ as a function of Π for $K = 0, 1, 1.5, 2, 2.5$ obtained when Eq.(1) is integrated with initial condition $s(0) = 0$ for Π increasing from 0 to 2 by 0.01 per time step $\Delta t^* = 0.1$, then decreasing to -1.9 , and finally increasing to 1.46. The result for $K = 0$ shows the classic hysteresis loop of the Stommel model. Much weaker hysteresis is obtained for $K = 1$, and it is shifted toward larger values of Π . Hysteresis occurs for $K \geq 1$ because of the discontinuity in the slope between the two stable modes at the bifurcation point. As K increases upward from unity the slopes of the two stable modes approach each other and the hysteresis disappears at about $K = 2.5$. This behavior is remarkably similar to the transition from the hysteresis loop simulated by the uncoupled OGCM (Figs. 8a and 8b) to the single curve simulated by the coupled AOGCM (Fig. 8c).

5. Conclusion

This study focuses on the reversibility/irreversibility of the THC after its shutdown, simulated by a hierarchy of climate models. Because the THC is most likely to slow down during this century, its dynamical behaviour is a very crucial issue and could result in different climate change policy. Simulations with an uncoupled 18-layer OGCM and with it coupled to an 11-layer AGCM have been carried out. The only significant difference between the uncoupled OGCM and the fully coupled AOGCM with respect to the THC simulation is the representation of the air-sea interaction. The results show that the shutdown of the THC is a reversible process in the fully coupled AOGCM simulation, whereas it is a irreversible process in the ocean-only model simulation. Additionally, the freshwater perturbation needed to shut down the THC is much larger in the AOGCM than in the uncoupled OGCM. There is no clear critical freshwater forcing that triggers an abrupt change of the THC intensity in the AOGCM simulations.

The different simulations of the dynamical behavior of the THC result from a crucial negative feedback in the AOGCM simulation which cannot occur in the uncoupled OGCM simulation. This feedback is closely related to the salinity advection within the upper ocean of the North Atlantic. After the shutdown of the THC, the upper ocean salinity over the low-latitude North Atlantic increases as a result of an enhanced evaporation there and a southward shift of the Atlantic ITCZ, both of which are related to the SST change over the Atlantic. The

southward shift of the Atlantic ITCZ results from a bipolar-seesaw pattern of the SST change after the shutdown of the THC. This change of SST, with cooling in the North Atlantic and warming in the South Atlantic, sends the annual-mean maximum P–E belt associated with the ITCZ from the North Atlantic into the South Atlantic. This facilitates the increase of the upper ocean salinity around the Caribbean Sea which is a critical region in regulating the intensity of the THC. Consequently, seawater with higher salinity is transported from the low-latitude Atlantic to the high-latitude Atlantic by the gyre and oceanic diffusion processes even after the THC shutdown. The high surface salinity is maintained over the northern North Atlantic, facilitating the resumption of deep convection after its cessation in the AOGCM simulation.

The salinity advection process in the ocean was originally regarded as a strong positive feedback process. However, the present study shows that after incorporating the air-sea interaction, the salinity advection could provide a negative feedback to stabilize the active THC or destabilize the inactive THC. The operation of the negative feedback identified in this study is through complex air-sea interactions. Without a detailed and comprehensive representation of the ocean-atmosphere system and their interaction, this feedback cannot be simulated.

Stommel's 2-box ocean model is the simplest possible way to study the dynamical behavior of the THC. The irreversibility of the THC after its shutdown was first demonstrated by this model. Whether or not a reversible shutdown of the THC can also occur within some parameter regime is of interest and importance. The Stommel/Saltzman 2-box ocean model (SSM) takes into consideration the contribution of the wind-driven gyre circulation and eddies to the mass exchange between the equatorial and polar boxes, which was neglected in Stommel's original version. It has been found that the dynamical behavior of the THC in the SSM is critically determined by a parameter K which is the ratio of the transport coefficient for the gyre circulation and eddies, k_{ϕ} , to that for the THC, k_{ψ} . The THC presents pronounced bistability, bifurcation, hysteresis and irreversibility with small values of K between zero and unity in the SSM. However, these nonlinear properties disappear when K takes values greater than unity. Therefore, the behavior of the THC

simulated by the uncoupled OGCM is like that of the SSM for small K , while the THC behavior simulated by the AOGCM is like that of the SSM for large K .

In the light of the behavior of the SSM for $K > 1$, what lesson should be learned from the OGCM and AOGCM simulations about the reversibility/irreversibility of the THC after its shutdown? It appears that the irreversible shutdown of the THC represented by the hysteresis loop of the OGCM simulations is an artifact of this model's not being able to simulate the negative feedback that occurs in the coupled AOGCM simulation, represented by large K in the SSM. However, we do not now know what the appropriate value of K is for the real ocean. Thus the possibility of an irreversible shutdown of the THC cannot be excluded altogether, hence policy options for such an occurrence should continue to be explored.

Acknowledgement

This material is based upon work supported by the National Science Foundation under Award No. ATM-0084270. Any opinions, findings, and conclusions or recommendations expressed in this publication are those of the authors and do not necessarily reflect the views of the National Science Foundation.

References

- Alley, R. B., J. Marotzke, W. D. Nordhaus, J. T. Overpeck, D. M. Peteet, R. A. Pielke, R. T. Pierrehumbert, P. B. Rhine, T. F. Stocker, L. D. Talley, and J. M. Wallace (2003), Abrupt climate change. *Science*, 299, 2005-2010.
- Arakawa, A. (1966), Computational design for long-term numerical integration of the equations of fluid motion: Two dimensional incompressible flow. Part I., *J. Computational Phys.*, 1, 119-143.
- Arakawa, A., and V. R. Lamb (1977), Computational design of the basic dynamical processes of the UCLA general circulation model, in *Methods in Computational Physics*, edited by J. Chang, Academic Press, New York, 173-265.
- Bryan, K., (1969), A numerical method for the study of the circulation of the world ocean. *J. Computational Phys.*, 4, 347-376.
- Chou, M. D., and M. J. Suarez (1994), An efficient thermal infrared radiation parameterization for use in General Circulation Models. *Technical Report Series on Global Modeling and Data Assimilation, National Aeronautical and Space Administration/TM-1994-104606*, 3, 85 pp.
- Cubasch, U *et al.* (2001), In *Climate Change 2001: The Scientific Basis*, J. T. Houghton *et al.* Eds., Cambridge Univ. Press, Cambridge.
- Curry, R., B. Dickson, and I. Yashayaev (2003), A change in the freshwater balance of the Atlantic Ocean over the past four decades. *Nature*, 426, 826-829.

- Delworth, T., S. Manabe, and R. J. Stouffer (1993), Interdecadal oscillation of the thermohaline circulation in a coupled ocean-atmosphere model. *J. Climate*, 6, 1993-2011.
- Dong, B. W. and R. T. Sutton (2002), Adjustment of the coupled ocean-atmosphere system to a sudden change in the thermohaline circulation. *Geophys. Res. Lett.*, 29, 18.1-18.4.
- Ganopolski, A. and S. Rahmstorf (2001), Rapid changes of glacial climate simulated in a coupled climate model. *Nature*, 409, 153 – 158.
- Ganachaud, A., and C. Wunsch (2000), Improved estimates of global ocean circulation, heat transport and mixing from hydrographic data. *Nature*, 408, 453-457.
- Han, Y.-J. (1984a), A numerical world ocean general circulation model, Part I. Basic design and barotropic experiment, *Dyn. Atmos. Ocean*, 8, 107-140.
- Han, Y.-J., A numerical world ocean general circulation model, Part II. A baroclinic experiment, *Dyn. Atmos. Oceans*, 8, 141-172, 1984.
- Johnson, H. L. and D. P. Marshall (2002), A theory for the surface Atlantic response to thermohaline variability. *J. Phys. Oceanogr.*, 32, 1121-1132.
- Latif, M. *et al.* (2000), Tropical stabilization of the thermohaline circulation in a greenhouse warming simulation. *J. Clim.*, 13, 1809-1813.
- Levitus, S., and T. P. Boyer (1994), World ocean atlas. U.S. Department of Commerce, Washington D.C..
- Manabe, S., and R. J. Stouffer (1988), Two Stable Equilibria of a Coupled Ocean-Atmosphere Model. *J. Clim.*, 1 (9), 841-866.
- Manabe, S. and R. J. Stouffer (1999), Are two modes of thermohaline circulation stable? *Tellus*, 51A, 400-411.
- Marotzke, J. and J. Willebrand (1991), Multiple equilibria of the global thermohaline circulation. *J. Phys. Oceanogr.*, 21, 1372-1385.
- Mikolajewicz and Maier-Reimer (1994), Mixed boundary conditions in ocean general circulation models and their influence on the stability of the model's conveyor belt, *J. Geophys. Res.*, 99, 22633-22644.

- Pacanowski, R. C., and S. G. Philander (1981), Parameterization of vertical mixing in numerical models of tropical ocean. *J. Phys. Oceanogr.*, *11*, 1443-1451.
- Prange, M., V. Romanova, and G. Lohmann (2002), Influence of vertical mixing on the thermohaline hysteresis: analyses of an OGCM. *J. Phys. Oceanogr.*, *33*, 1707-1721.
- Rahmstorf, S. (1995), Bifurcations of the Atlantic thermohaline circulation in response to changes in the hydrological cycle. *Nature*, *378*, 145-149.
- Rind, D. *et al.* (2001), Effects of glacial meltwater in the GISS coupled atmosphere-ocean model, *J. Geophys. Res.*, *106*, 27335-27353.
- Saltzman, B. (2002), Dynamical Paleoclimatology 206-231.
- Schiller, A., U. Mikolajewicz, and R. Voss (1997), The Stability of the North Atlantic thermohaline circulation in a coupled ocean-atmosphere general circulation model, *Clim. Dyn.*, *13*, 325-347.
- Schlesinger, M. E. *et al.* (1985), The role of the ocean in CO₂-induced climatic warming: Preliminary results from the OSU coupled atmosphere-ocean GCM, in *Coupled Ocean-Atmosphere Models*, edited by J.C.J. Nihoul, pp. 447-478, Elsevier, Amsterdam.
- Schlesinger, M. E. *et al.* (1997), Progress report for the second year of NSF/DOE grant ATM 95-22681.
- Schmidt, M. W., H. J. Spero, and D. W. Lea (2004), Links between salinity variation in the Caribbean and North Atlantic thermohaline circulation. *Nature*, *428*, 160-163.
- Schmittner, A. and A. J. Weaver (2001), Dependence of multiple climate states on ocean mixing parameters. *Geophys. Res. Lett.*, *28*, 1027-1030.
- Schmittner, A., M. Yoshimori, and A. J. Weaver (2002), Instability of glacial climate in a model of ocean-atmosphere-cryosphere system. *Science*, *295*, 1489-1493.
- Stocker, T., and D. Wright (1991), Rapid transitions of the ocean's deep circulation induced by changes in surface water flux, *Nature*, *351*, 729-732.
- Stommel, H. M. (1961), Thermohaline convection with two stable regimes of flow, *Tellus*, *13*, 224-230.

- Titz, S. *et al.* (2002), On freshwater-dependent bifurcation in box model of the interhemispheric thermohaline circulation. *Tellus*, 54A, 89-98.
- Vellinga, M. and R. Wood (2002), Global climatic impacts of a collapse of the Atlantic thermohaline circulation. *Climatic Change*, 54, 251-267.
- Vellinga, M., R. A. Wood, and J. M. Gregory (2002), Processes governing the recovery of a perturbed thermohaline circulation in HadCM3. *J. Clim.*, 15, 764-780.
- Wang, W., and M. E. Schlesinger, 1995: The dependence on convective parameterization of tropical intraseasonal oscillations - an assessment using the UIUC GCM. *Proceedings of the First International AMIP Scientific Conference, Monterey, California, USA, 15-19 May 1995*, WMO WCRP-92, WMO/TD-No. 732, Geneva, 125-130.
- Yang, F. (2000), Radiative forcing and climatic impact of the mount Pinatubo volcanic eruption. Ph. D. dissertation, University of Illinois, Urbana-Champaign, 218 pp.

Figure Captions

Figure 1. The ocean currents in the Atlantic Ocean simulated by the UIUC coupled atmosphere/ocean general circulation model (50-year mean). Unit: cm/s. a: upper ocean (mean of 0-1000 m); b: deep ocean (mean of 1000-3000 m).

Figure 2. Two vertical cross-sections in the Atlantic Ocean simulated by the UIUC AOGCM (50-year mean). Positive values (shaded) mean northward flow. Unit: cm/s a: 30°N; b: 50°N.

Figure 3. The geographical distribution of SST. (a) Observation [Levitus *et al.*, 1994]; (b) Simulation by the UIUC AOGCM (50-year mean); (c) Difference between the simulation and the observation. Unit: °C. Temperatures greater than 26°C are shaded in panels a and b. Negative values are shaded in panel c.

Figure 4. The geographical distribution of SSS. (a) Observation [Levitus *et al.*, 1994]; (b) Simulation by the UIUC AOGCM (50-year mean); (c) Difference between the simulation and the observation. Unit: p.s.u.. Salinities greater than 36.5 p.s.u. are shaded in panels a and b. Negative values are shaded in panel c.

Figure 5. The time series of the global-mean root-mean-square difference between the simulated and observed SST and SSS.

Figure 6. The time-dependent freshwater perturbation in the uncoupled OGCM experiments. The freshwater perturbation changes linearly at a rate of 0.2 Sv per 1000 years.

Figure 7. The freshwater perturbation experiments using the coupled AOGCM. (a) the first group; (b) the second group.

Figure 8. The stability diagrams of the THC established by the uncoupled OGCM and coupled AOGCM. (a) The OGCM with prescribed surface heat and salinity fluxes; (b) The OGCM with prescribed salinity flux and calculated heat flux (mixed boundary condition); (c) The AOGCM (50-year mean). Red, blue and green colors represent the increase in freshwater addition, the subsequent decrease in freshwater addition after the THC is shut down, and the following increase in freshwater addition. The origin of the x axis represents the “present-day” freshwater flux. The rectangles indicate the equilibrium runs with the uncoupled OGCM. The red points in (c) with the same freshwater forcing come from different groups. The red dashed line is the linear fit based on the red points.

Figure 9. The evolution of the meridional mass streamfunction in the uncoupled OGCM with prescribed fluxes (left panels) and in the AOGCM (right panels). The first number on the top left is the freshwater forcing for the initial condition and the second number is freshwater forcing in the experiment. Both values are relative to the control run.

Figure 10. A T-S diagram showing the responses of SST and SSS over 50-70°N of the North Atlantic to different freshwater perturbations. The values are 50-year means. The numbers beside the marks indicate the freshwater perturbations. Red: the AOGCM; Blue: the uncoupled OGCM with prescribed fluxes; Green: the uncoupled OGCM with mixed boundary conditions. Contours are potential density σ_t in kg/m^3 .

Figure 11. The change in salinity (parts per thousand) of the upper ocean (100 m) after the THC is shut down together with the upper ocean wind-driven circulation (cm/s). (a) 0.2 Sv freshwater perturbation in the OGCM with prescribed heat and salinity fluxes. (b) 0.6 Sv freshwater perturbation in the AOGCM.

Figure 12. The changes of (a) precipitation (P), (b) evaporation (E) and (c) P–E after the THC shutdown in the AOGCM simulation. Unit : mm/day.

Figure 13. The zonally averaged salinity change after the shutdown of the THC. (a) 0.2 Sv freshwater perturbation in the uncoupled OGCM with prescribed fluxes; (b) 0.2 Sv perturbation in the uncoupled OGCM with mixed boundary condition; (c) 0.6 Sv freshwater perturbation in the AOGCM.

Figure 14. The THC intensity $\Psi/k_{\psi}\mu_T\delta T^* = (1-s)$ as a function of the external freshwater forcing Π in the Stommel/Saltzman two-box ocean model. (a) Equilibrium solutions $s^{(1)}$, $s^{(2)}$ and $s^{(3)}$ as a function of the external freshwater forcing Π for $K = 0, 1, 1.5, 2, 2.5$. (b) Hysteresis curves constructed by varying the freshwater forcing Π .

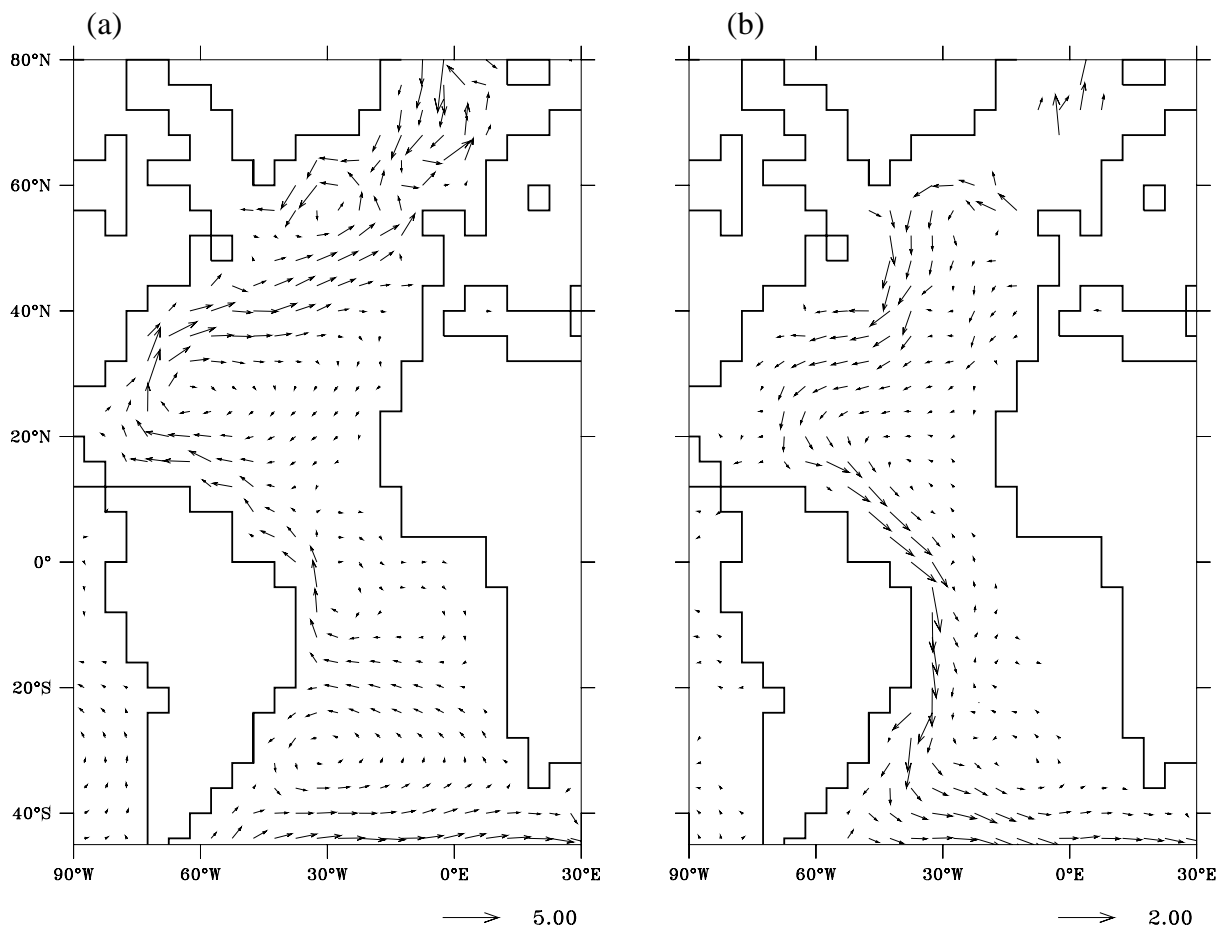


Figure 1.

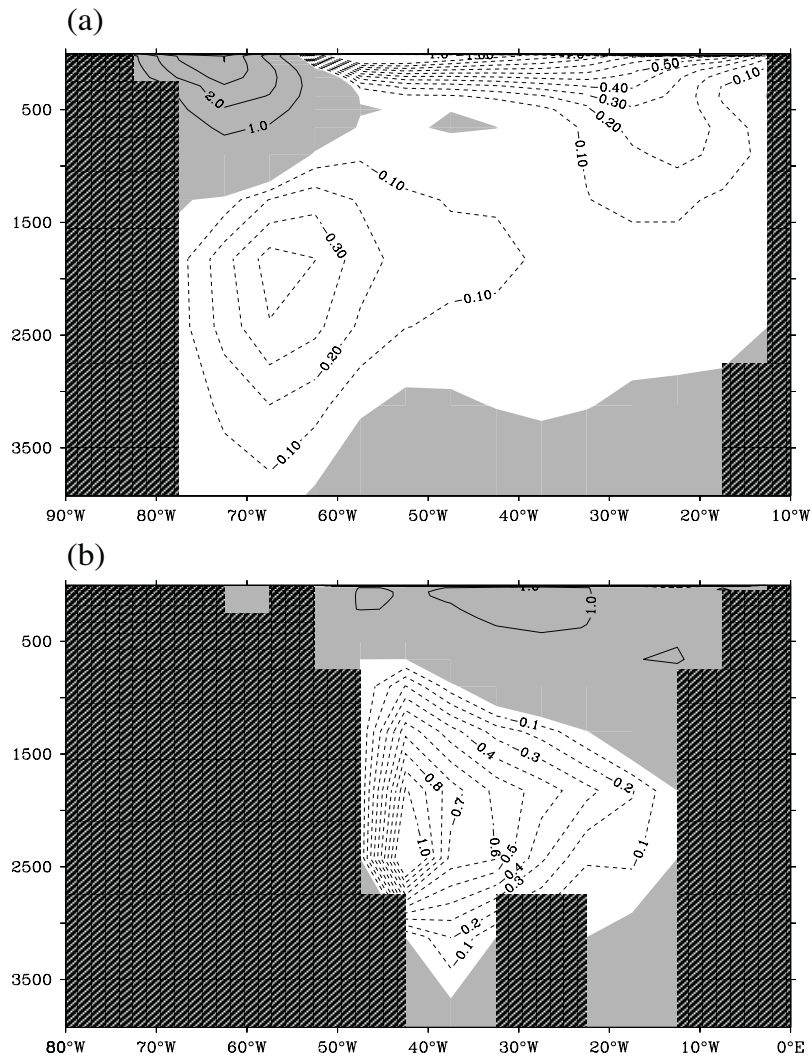


Figure 2.

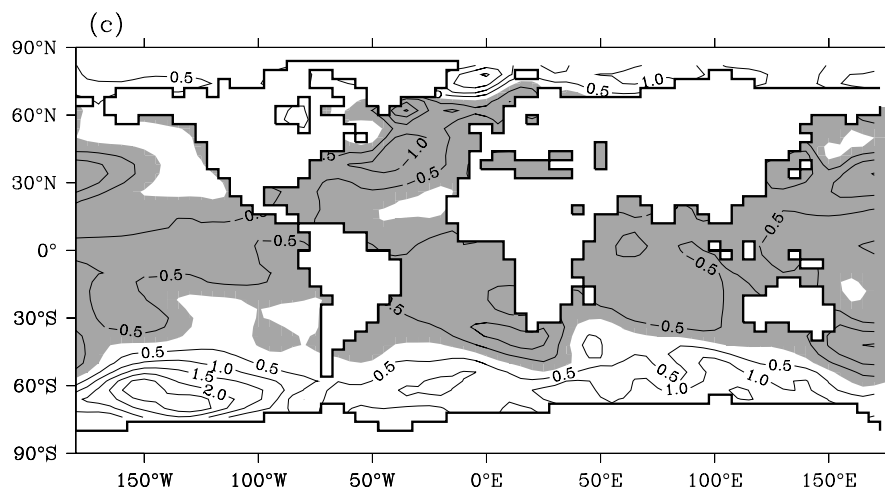
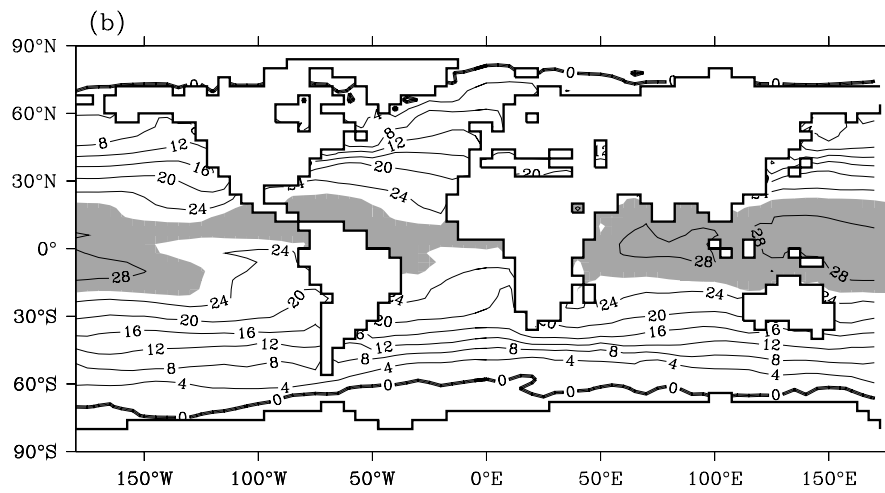
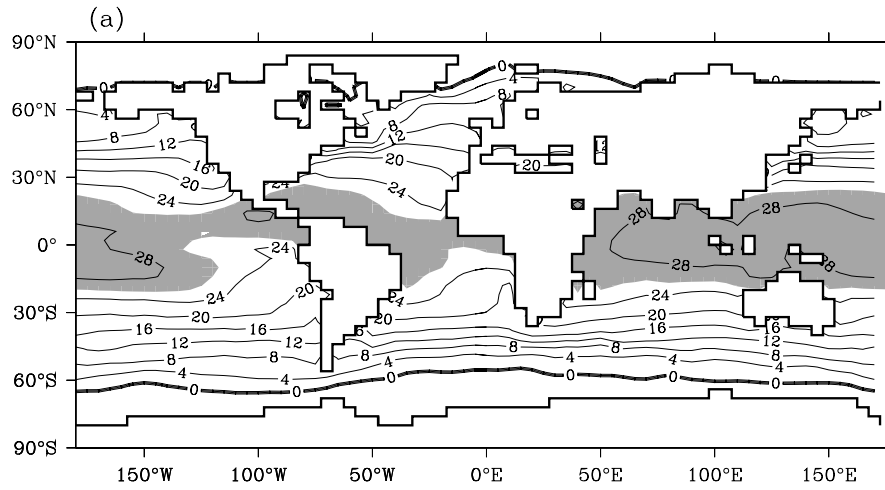


Figure 3.

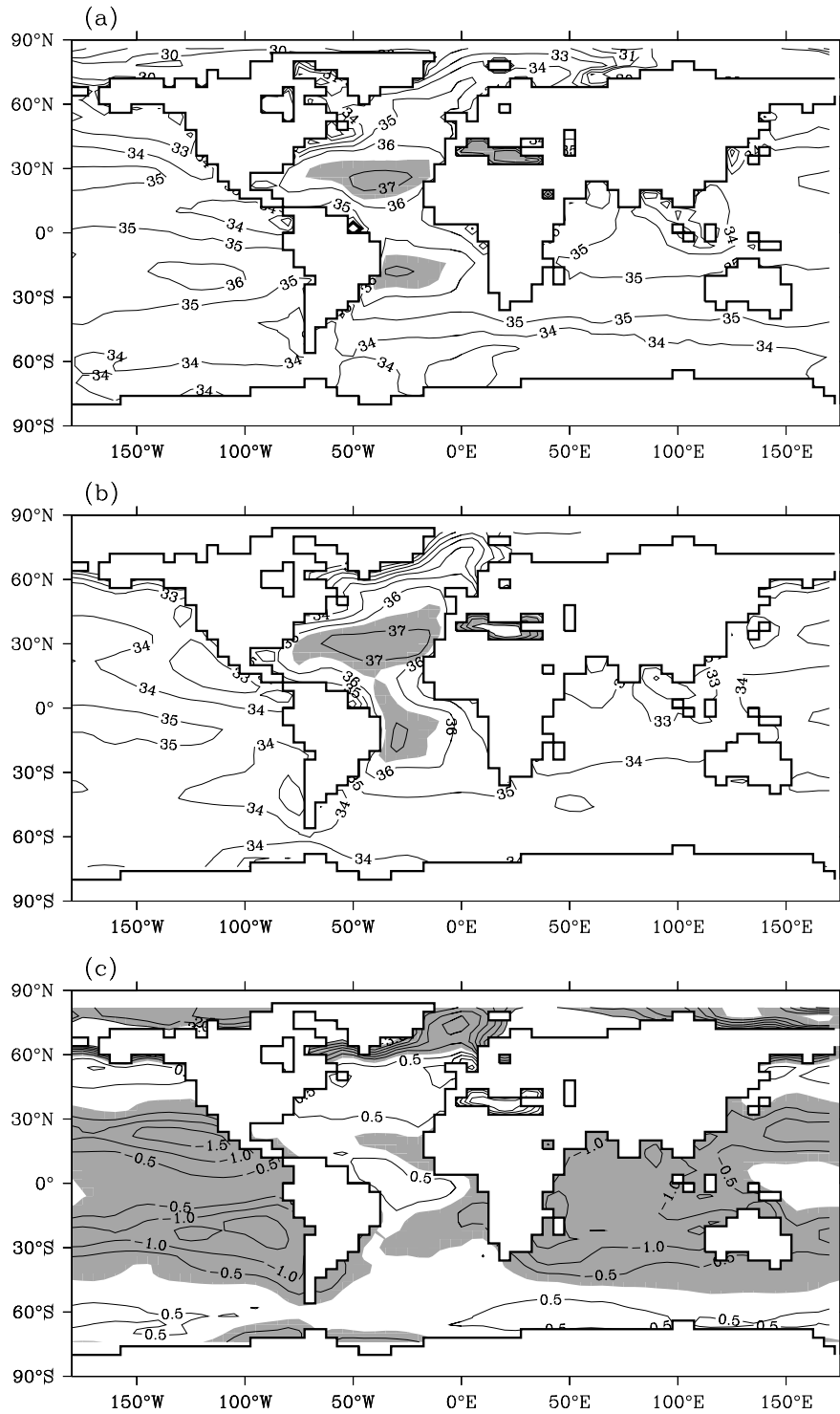


Figure 4.

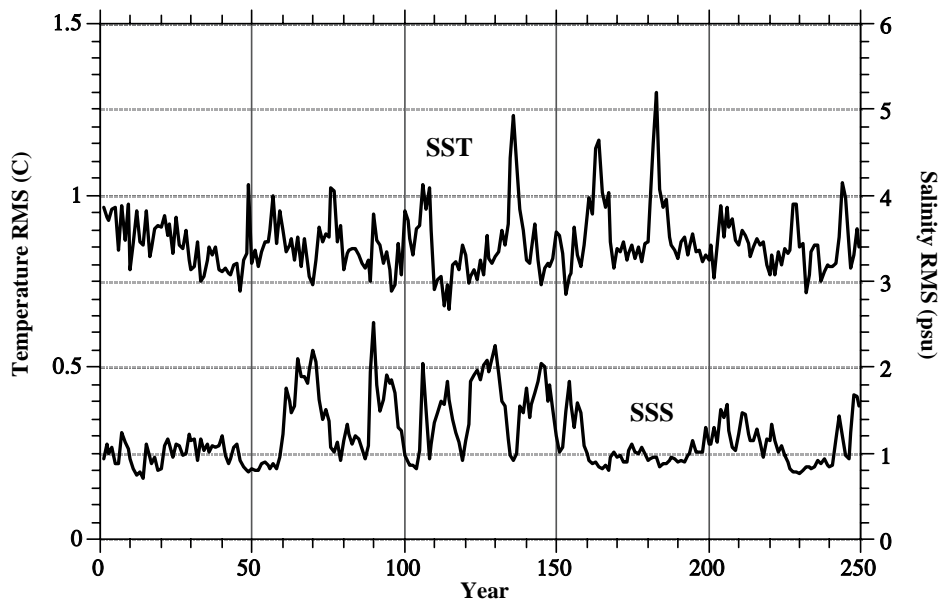


Figure 5.

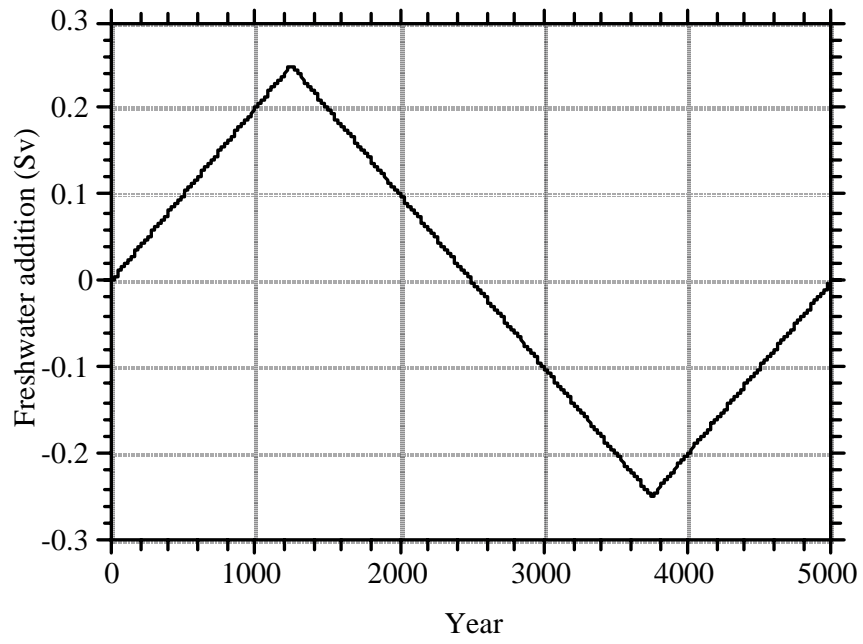


Figure 6.

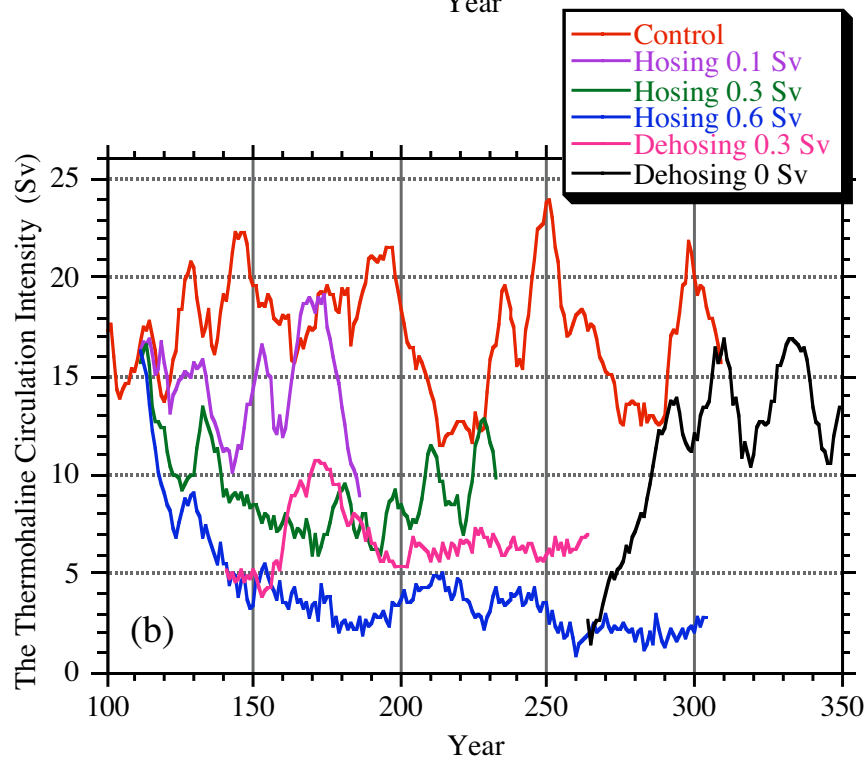
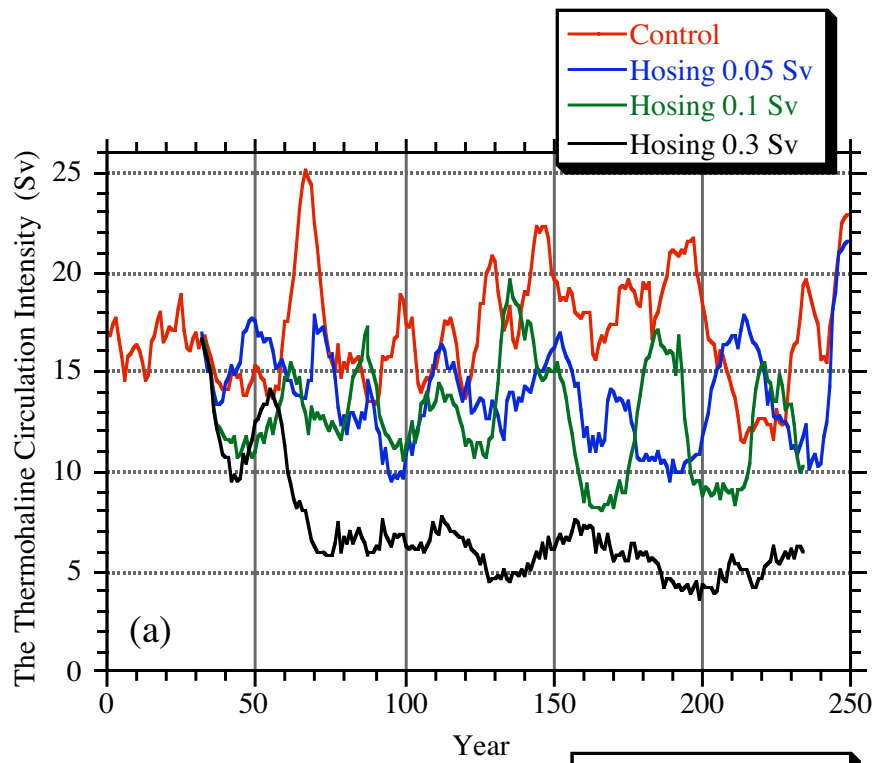


Figure 7.

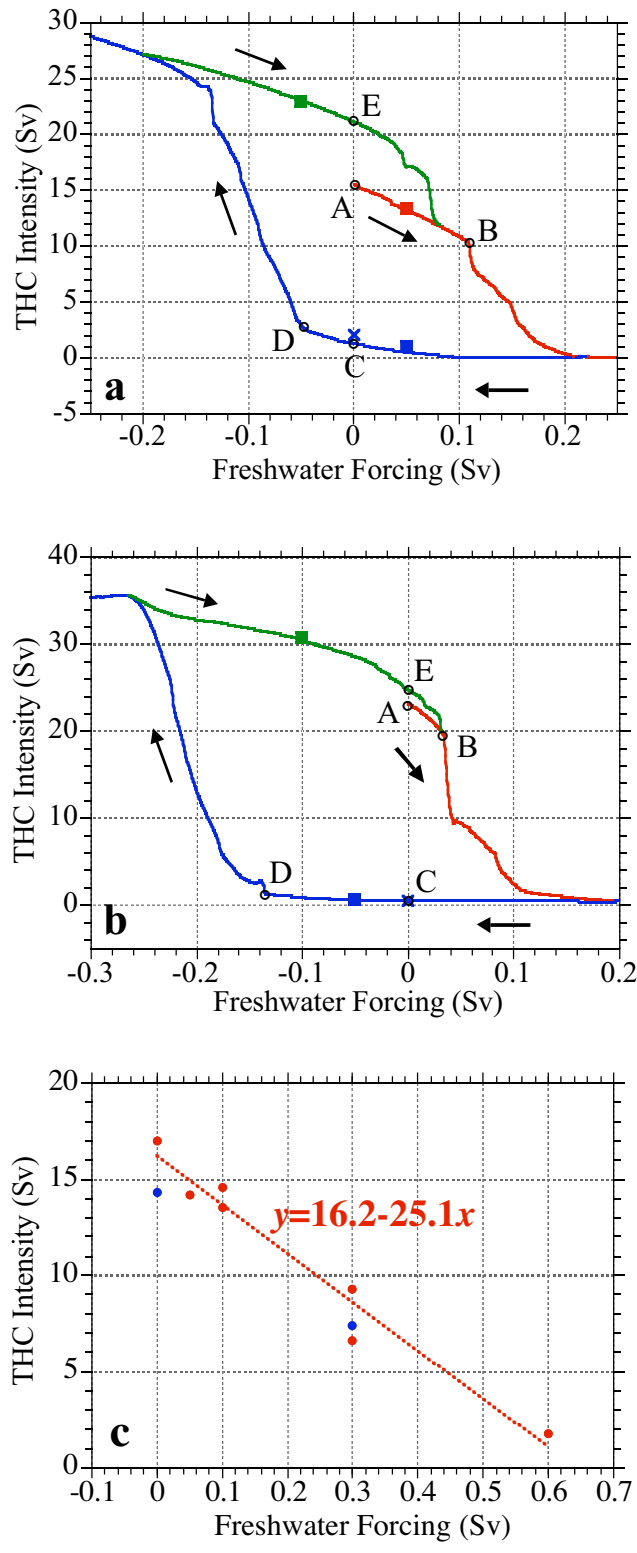


Figure 8.

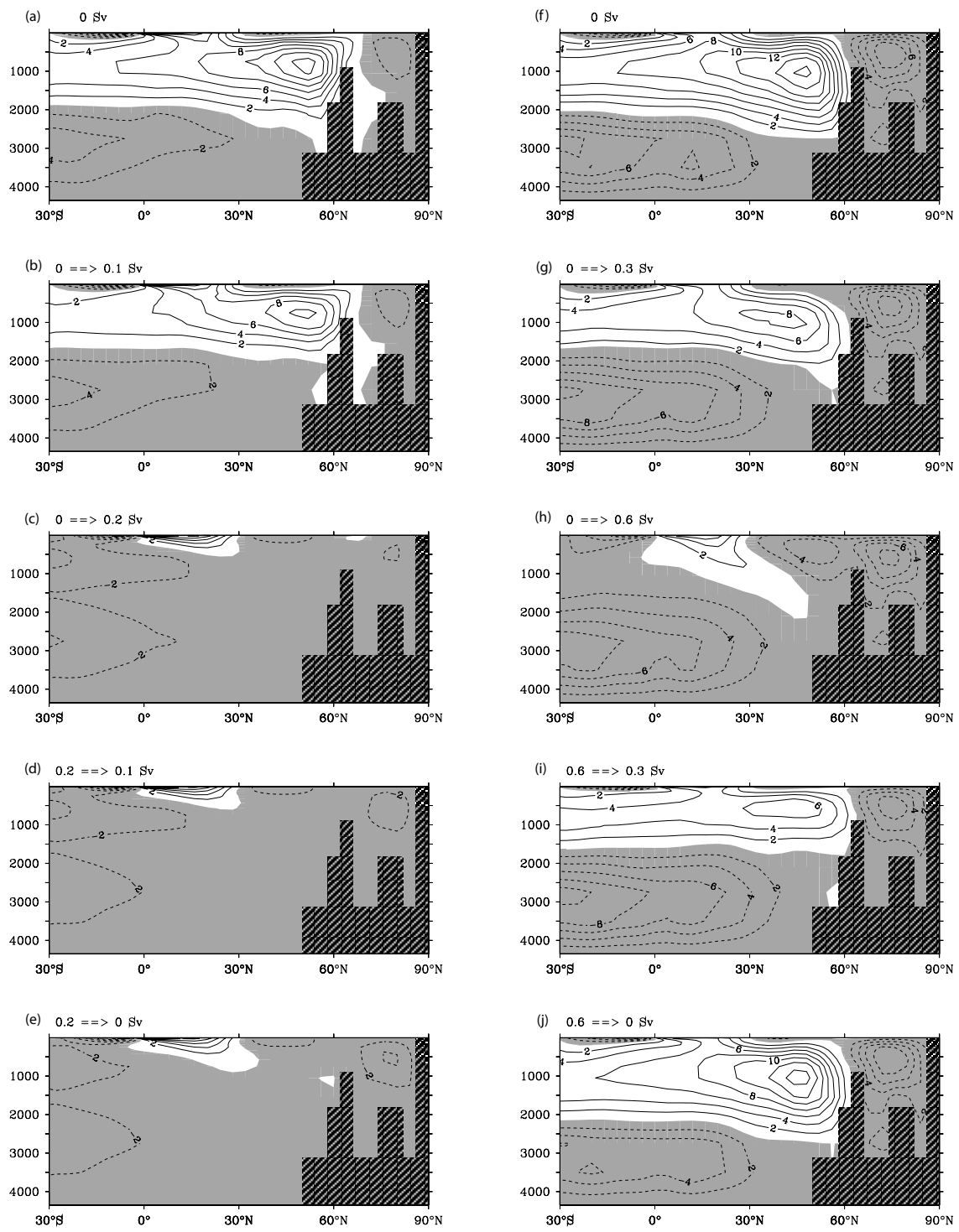


Figure 9.

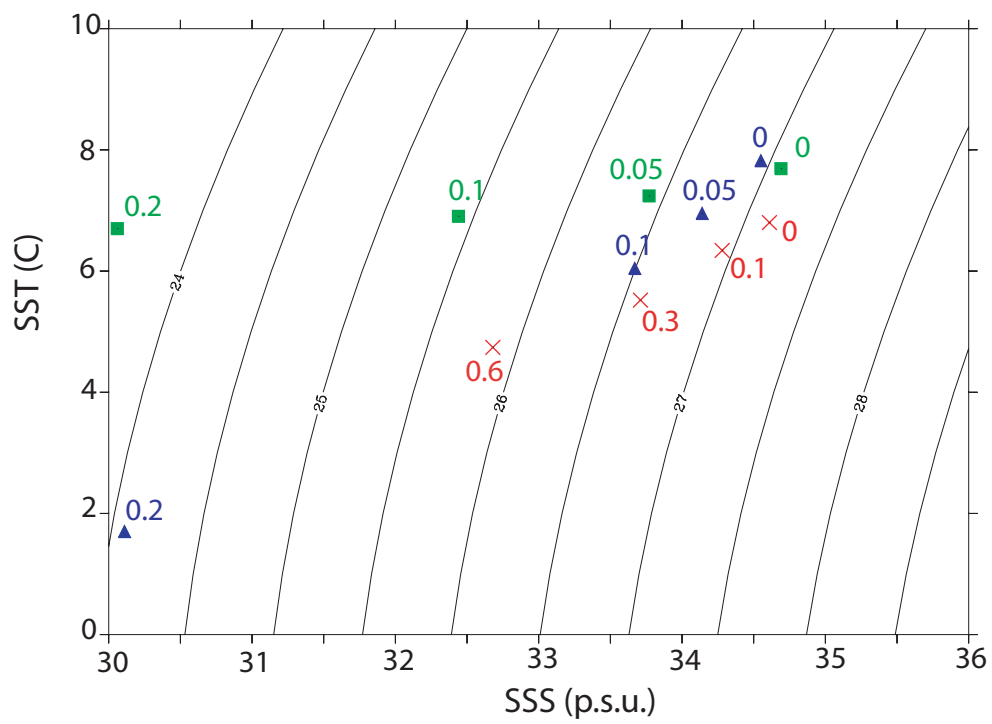


Figure 10.

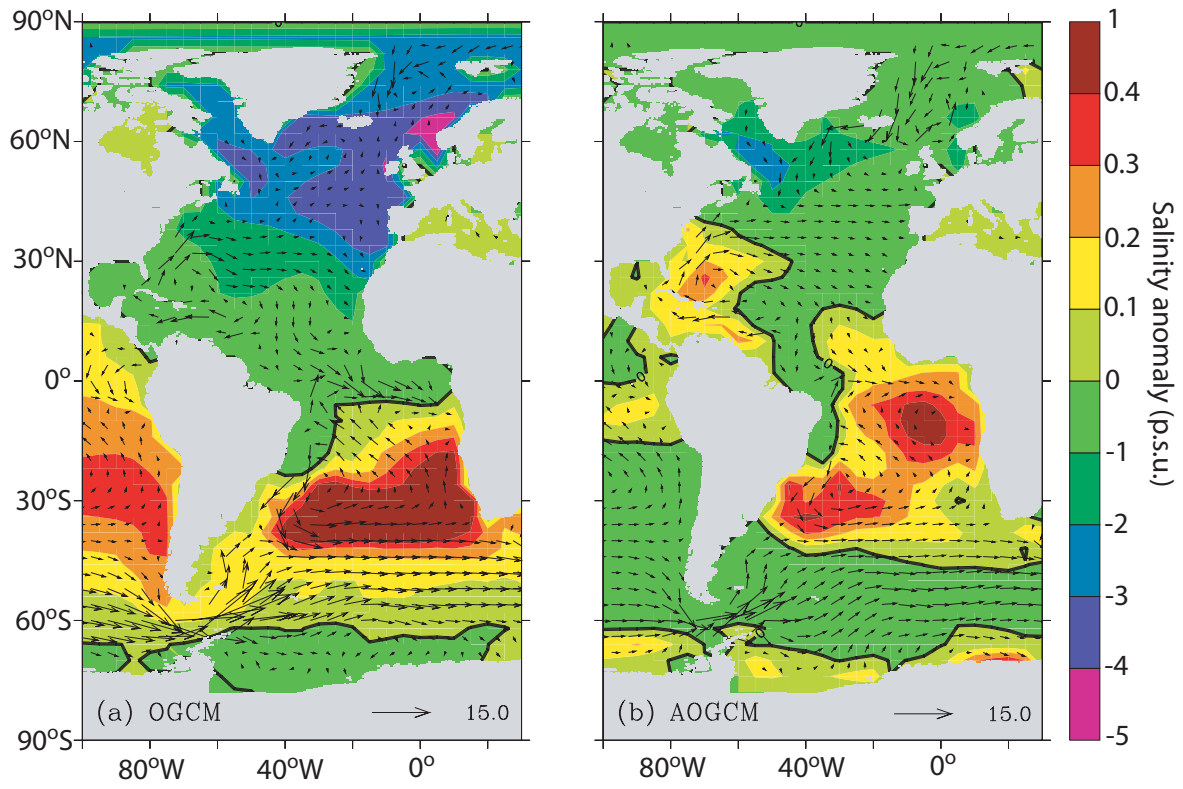


Figure 11.

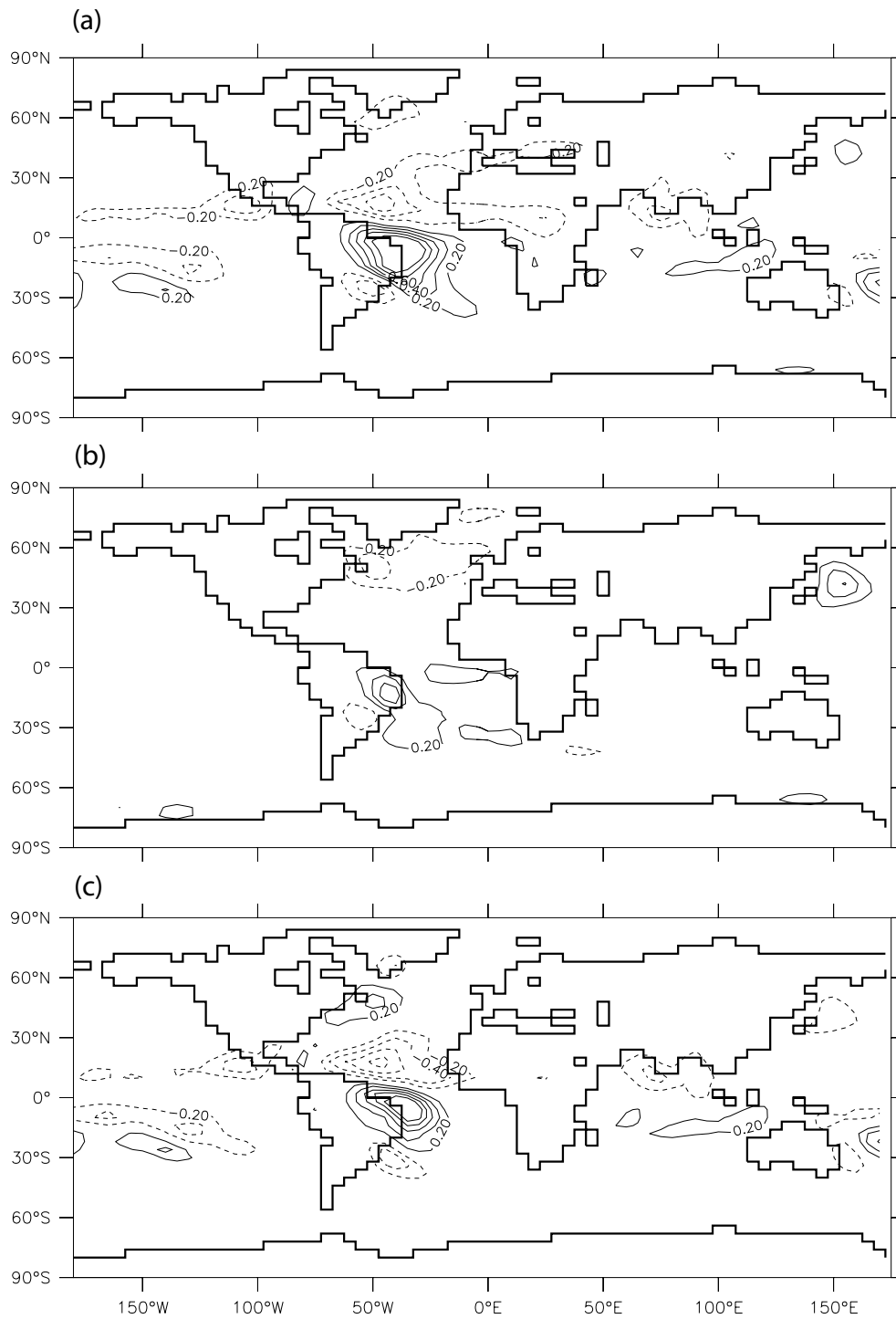


Figure 12.

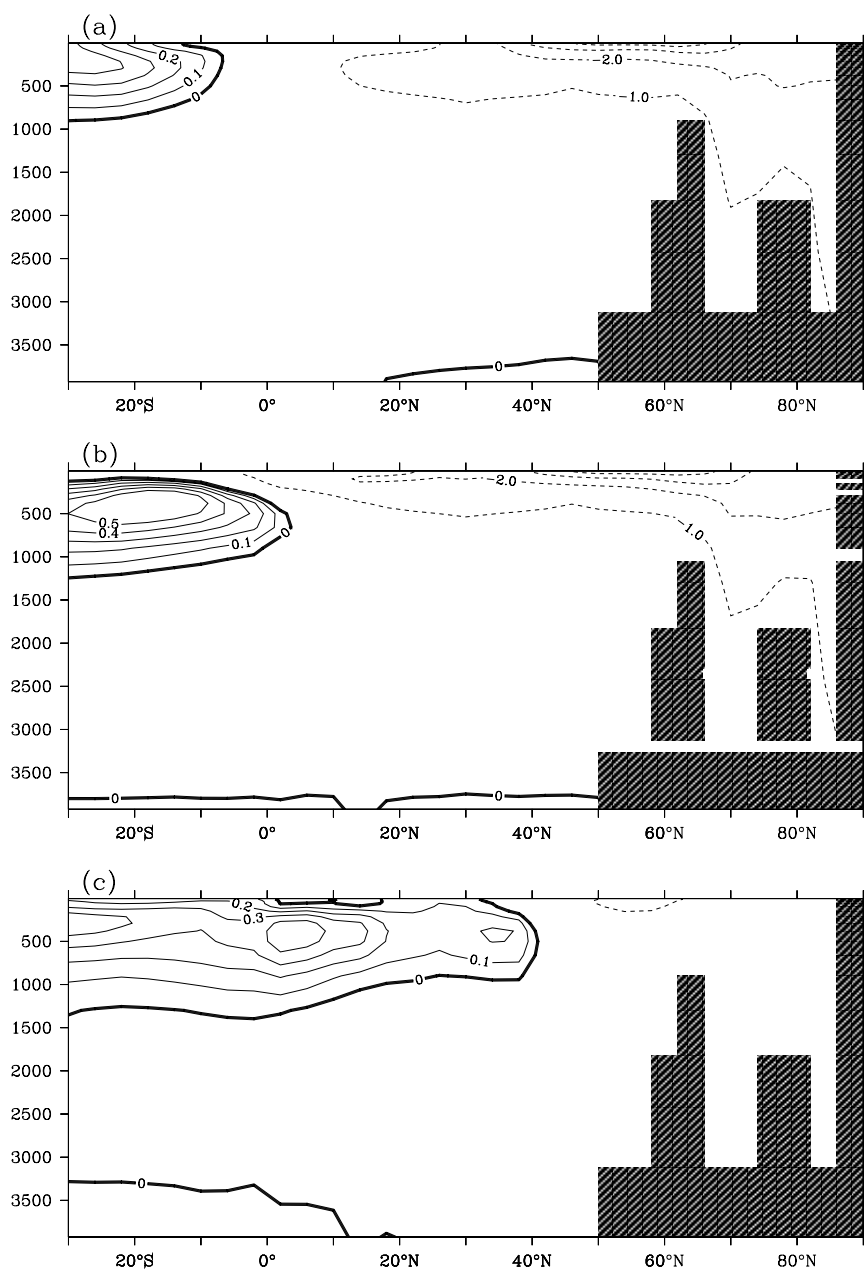


Figure 13.

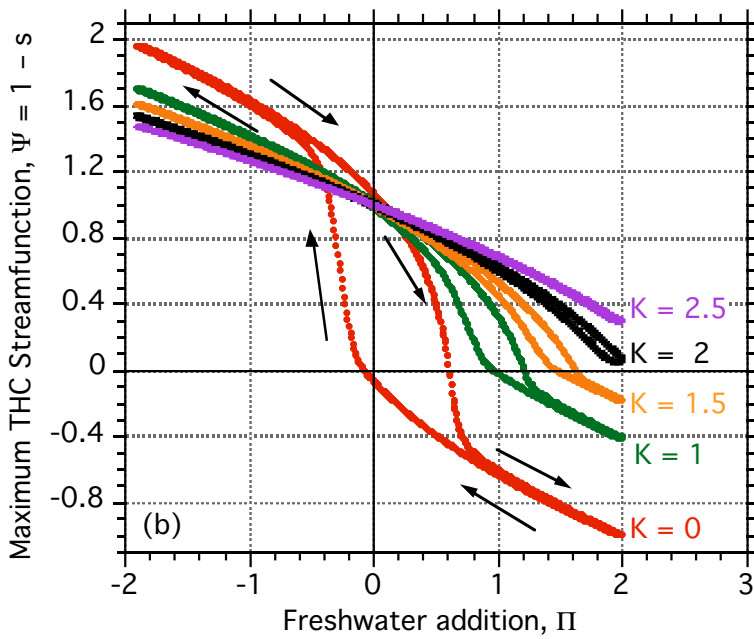
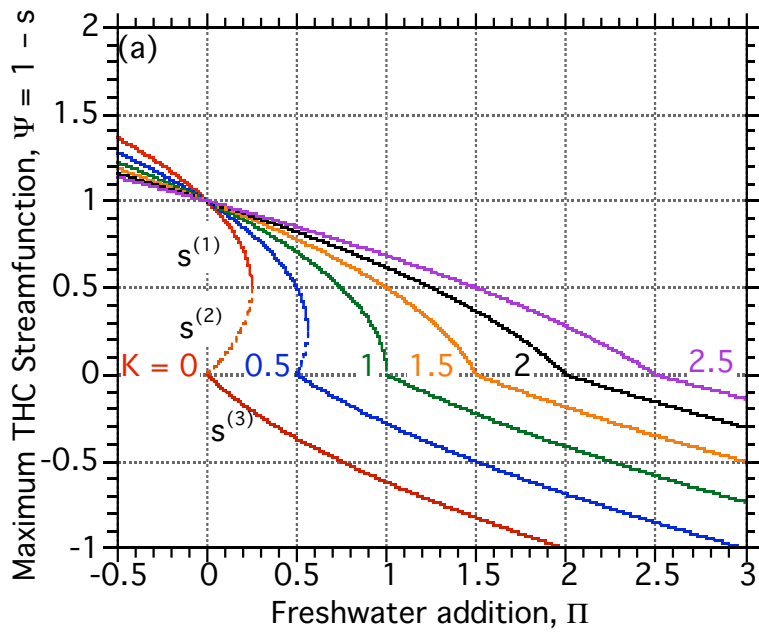


Figure 14.